Chin. Sci. Bull. (2014) 59(14):1485–1491
DOI 10.1007/s11434-014-0215-8

csb.scichina.com
www.springer.com/scp

Article

Atmospheric Science

Effects of spectral sampling rate and range of CO_2 absorption bands on XCO_2 retrieval from TanSat hyperspectral spectrometer

Yi Liu · Zhaonan Cai · Dongxu Yang · Yuquan Zheng · Minzheng Duan · Daren Lü

Received: 17 July 2013 / Accepted: 14 August 2013 / Published online: 11 March 2014

Abstract The spectral sampling rate and range of CO_2 absorption bands are critical for the optimal design of hyperspectral instrument for CO_2 observation satellite. Undersampling of spectra in space-based spectrometer significantly contaminates signals measured in the CO_2 1.61 μm-band. The CO_2 dry-air column (XCO_2) error due to spectral undersampling can be up to ~1 ppm, which is the target precision of the Chinese Carbon Satellite (TanSat) for a single sounding. Undersampling error depends on surface albedo, solar zenith angle, and scattering properties in the atmosphere. The spectral sampling rate is recommended to be greater than 2.0 pixels per full width at half maximum to avoid undersampling. Reduction of spectral resolution and the use of narrower spectral regions can improve spectral sampling with little changes in CO_2 retrieval sensitivity without losing much information. The full-band approach provides direct constraints on the wavelength-dependent surface albedo and particle scattering from the measurements. To keep a broader band, we recommend reduction of the spectral resolution by a factor of two.

Keywords XCO_2 · TanSat · Spectral sampling · Band selection · Hyperspectral spectrometer

SPECIAL TOPIC: Greenhouse Gas Observation From Space: Theory and Application

Y. Liu · Z. Cai (✉) · D. Yang · M. Duan · D. Lü
Key Laboratory of Middle Atmosphere and Global Environment Observation, Institute of Atmospheric Physics, Chinese Academy of Sciences, Beijing 100029, China
e-mail: caizhaonan@mail.iap.ac.cn

Y. Zheng
Changchun Institute of Optics, Fine Mechanics and Physics, Chinese Academy of Sciences, Changchun 130033, China

1 Introduction

Carbon dioxide (CO_2) is an important greenhouse gas in the atmosphere. In order to characterize sources and sinks on regional scales, space-based global measurements of atmospheric CO_2 with adequate precision, resolution, and coverage are needed. Several hyperspectral instruments have been launched, such as the scanning imaging absorption spectrometer for atmospheric chartography (SCIAMACHY) and the greenhouse gases observing satellite (GOSAT). Satellites yet to be launched include the orbiting carbon observatory-2 (OCO-2) and the Chinese CO_2 observation satellite (TanSat), as well as the proposed CarbonSat. To improve the sensitivity to CO_2 variability in the lower troposphere, these space-based instruments measure backscattered and reflected sunlight in near-infrared CO_2 absorption bands.

SCIAMACHY, with spectral coverage over near-infrared CO_2 bands, was launched on the Envisat in 2002 [1] and is an eight-channel grating spectrometer. GOSAT was launched into orbit in 2009 [2]. The thermal and near-infrared sensor for carbon observation on board GOSAT is a Fourier transform spectrometer that observes the wide spectrum range of light from short-wavelength infrared using interference phenomena. OCO-2 carries a single instrument that incorporates three long-slit-imaging grating spectrometers optimized for O_2-A band (0.76 μm) and two CO_2 bands (1.61 and 2.06 μm). OCO-2 will be launched in late 2014 [3]. The TanSat is the first mission of China's Ministry of Science and Technology dedicated to monitoring CO_2 from space and is planned for launch in 2015. The CO_2 Sensor on board the TanSat is designed to be similar to OCO-2 in band selection but different in instrument characterization. TanSat uses three gratings and a two-dimensional CCD detector array, with 20 cross-track

positions in different rows and dispersed spectra in different columns.

Column-averaged dry-air mole fractions of CO_2 (XCO_2) can be retrieved from measured Earth-viewing radiance measurements normalized by irradiance. In order to fit spectra, it is usually necessary to resample a measured solar spectrum to a radiance wavelength grid, because of a relative wavelength shift between measured solar irradiance (F) and Earth-viewing radiance (I) [4]. Several retrieval algorithms have been developed to retrieve XCO_2 from SCIAMACHY and GOSAT measurements. These algorithms are physically based on [3, 6–8], except for the photon path length probability density function method [5]. These algorithms use a solar model, which is based on an empirical solar lines list, in the radiative transfer calculation [6]. This method avoids resampling of the solar spectrum, but may introduce artificial errors due to imperfect high-resolution solar reference spectrum and inconsistent radiometric calibration between empirical irradiance and measured radiance. It is more favorable to use the measured solar spectrum to cancel the radiometric calibration errors that are common in radiance and irradiance. For OCO-2 and TanSat, the solar spectra will typically be acquired once per day at the terminator in the Northern Hemisphere. The solar reference spectrum will be derived from this mode. OCO-2 and TanSat are grating- and array-based spectrometers that can suffer substantially from spectral undersampling because the I/F wavelength shift often occurs when there are Doppler and thermally introduced shifts. OCO-2 (CarbonSat) is currently designed to have more than 2.6(3) samples per full width at half maximum (FWHM), which will be sufficiently oversampled, as demonstrated by [4]. For the TanSat preliminary configuration, the spectral sampling rates (i.e., the ratio of spectral resolution and spectral interval) are currently designed to be higher than 2.0, 1.0, and 1.0 in the O_2-A, CO_2-weak, and CO_2-strong bands, respectively (Table 1). As a consequence, for the worst case, the TanSat spectrometer may suffer significantly from spectral undersampling (i.e., not satisfy the Nyquist sampling criterion).

In this paper, we evaluate the effects of the spectra undersampling rate and range on XCO_2 retrievals based on high-resolution solar spectra database and synthetic TanSat measurements, and provide suggestion to avoid undersampling error in instrument characterizations.

2 Synthetic undersampling spectra and TanSat measurements

2.1 Undersampling spectra calculation

Following the method described by Chance et al. [4], the undersampling effect can be simulated from the instrument line shape (ILS) (i.e., slit function) and the synthetic TanSat irradiance measurement. We assume Gaussian slit functions with FWHM of 0.081 and 0.103 nm for CO_2 weak (1.61 μm) and strong bands (2.06 μm), respectively. The FWHM values are from the preliminary instrument configuration [9]. Synthetic TanSat irradiance measurement is simulated by convolving the high-spectral-resolution solar spectrum with TanSat slit functions to the TanSat resolution and resampling onto the TanSat wavelength grid. The original high-resolution solar spectrum used for the present purpose is from a version that was developed for GOSAT (http://kurucz.harvard.edu/sun/). The irradiance spectrum was sampled at an increment less than 0.002 nm. Figure 1 shows the solar spectrum in high resolution and in TanSat resolution at 1,594–1,624 and 2,042–2,082 nm. There are many more solar Fraunhofer lines on the black-body continuum in a short-wavelength window than in the longer wavelength window. Radiance observed by TanSat in these bands will be normalized by irradiance and be used to retrieve XCO_2 as well as auxiliary states such as water-vapor column scaling, temperature offset, surface albedo, and aerosol optical depth [9, 10].

Calculation of a synthetic undersampling effect is accomplished following the method proposed by Chance et al. [4]. We review some of the basics here, please refer to the original publication for more details. The calculation of undersampling optical depth $\tau_u(\lambda)$ includes: (1) convolving the high-resolution solar reference spectrum with ILS to create a lower resolution oversampled solar reference spectrum F_{over}, as shown in Fig. 1; (2) creating a pseudo wavelength grid for irradiance λ_{irr} and radiance λ_{rad} with a relative wavelength shift of $\Delta\lambda$; (3) sampling F_{over} at the wavelength grids λ_{irr} and λ_{rad} to give the correct but undersampled solar reference spectrum F_{irr} and F_{rad}; (4) interpolating F_{irr} onto λ_{rad}, to give $F'_{rad}(\lambda)$; and (5) $\tau_u(\lambda)$ is given by

Table 1 TanSat preliminary instrument configuration for CO_2 weak and strong bands

Band	Band range (nm)	FWHM (nm)	Spectral interval (nm)	SNR/reference energy (photons s^{-1} cm^{-2} sr^{-1} nm^{-1})
CO_2-1.61	1,594–1,624	0.081	0.081	$250/2.1 \times 10^{12}$
CO_2 -2.06	2,042–2,082	0.103	0.103	$180/1.1 \times 10^{12}$

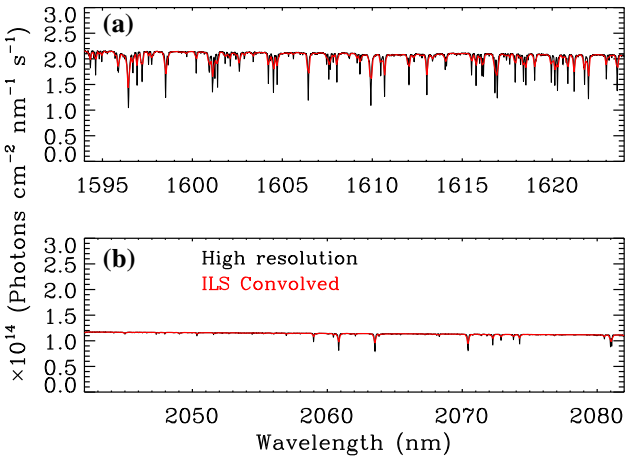

Fig. 1 High resolution (*black*) and low resolution convolved with the TanSat instrument line shape (*red*) solar spectrum in the CO_2 1.61 (**a**) and 2.06 μm (**b**) band

$$\tau_u(\lambda) = \frac{F_{rad}(\lambda) - F'_{rad}(\lambda)}{F_{rad}(\lambda)}. \quad (1)$$

The magnitude of $\tau_u(\lambda)$ depends on $\Delta\lambda$ and the position and strength of the solar lines. The $\Delta\lambda$ are due to Doppler and thermal effects. The Doppler shift is caused by velocity difference between the solar measuring mode and Earth-viewing mode. The velocity of a satellite when it flies toward the Sun across the terminator over the North Pole is about 7 km s^{-1}. The Doppler shift can be corrected systematically, and there is still some residual shift due to the ellipticity of the Earth's orbit. The thermally induced shift is difficult to correct because the thermal control uncertainty is attributed to the difference between solar mode and Earth-viewing mode: the former operates when the satellite flies over the northern terminator from the dark side of orbit to the bright side, whereas the latter is operating on the bright side. Figure 2 shows an example of $\tau_u(\lambda)$ when $\Delta\lambda$ is assumed to be 0.001 and 0.008 nm, for the two CO_2 bands. It is straightforward to give a first evaluation of the undersampling effect by comparing $\tau_u(\lambda)$ with 0.3 %–1 % CO_2 optical depth (equivalent to 1–4 ppm CO_2 change, the precision target of TanSat). In CO_2-weak band, $\tau_u(\lambda)$ increases substantially with increasing $\Delta\lambda$. Undersampling (one sample) can significantly contaminate CO_2 signals. It should be noted that the value of 0.008 nm is assumed to be the spectral calibration precision (one tenth of FWHM) of the TanSat preliminary configuration. The shift in flight is still unknown and may be larger than can be accounted for by Doppler shift correction. $\tau_u(\lambda)$ becomes much smaller when there are two samples per FWHM, either reducing the spectral sampling interval by half while keeping FWHM or increasing the FWHM by a factor of 2 while keeping spectral sampling rate. For CO_2-strong band, $\tau_u(\lambda)$ is negligible compared with CO_2 optical depth, because there are fewer solar lines in this wavelength region and stronger CO_2 absorption than from a decoupling of the weak band.

2.2 XCO_2 error due to undersampling

To address the XCO_2 retrieval error due to the undersampling effect, we use the retrieval simulation system that has been developed for TanSat [10]. We calculate synthetic TanSat Sun-normalized radiance and weighting functions with respect to surface albedo, trace gas (CO_2, water vapor, CH_4) absorption, temperature, surface pressure, and aerosol optical depth using the vector linearized discrete ordinate radiative transfer model (VLIDORT) under various Lambertian surface albedos. We use the optimal estimation technique to calculate the gain matrix G_y and postcovariance matrix S_m from the a priori covariance matrix S_a, measurement error S_ε, and weighting functions for each simulation. The state vector contains partial CO_2 columns in 24 layers, first-order polynomial in wavelength dependence of surface albedo, a water-vapor scaling factor, a temperature scaling factor, and the aerosol optical depth. The gain matrix is given by

$$G_y = \left(K^T S_\varepsilon K + S_a^{-1}\right)^{-1} K^T S_\varepsilon^{-1}. \quad (2)$$

For undersampling error, the posterror covariance can be expressed as

$$\hat{S}_m = G_y S_m G_y^T, \quad (3)$$

in which the gain matrix G_y describes the sensitivity of retrieved states (here for CO_2 elements only) to measurements, and S_m represents the undersampling error covariance matrix in the logarithm of Sun-normalized radiance, the diagonal elements are τ_u^2 in Eq. (1). Here, we take the logarithm, in order to reduce the nonlinearity in the inverse model. The bias in XCO_2 can be expressed as $\Delta XCO_2^2 = (h^T \hat{S}_m h)$, where h is the air column vector.

Figure 3a shows the retrieval error (ΔXCO_2) in the retrieved XCO_2 (1.61-μm band only retrievals) due to undersampling, random noise error in the simulated measurements in the Rayleigh scattering only condition. The random noise error decreases with increasing surface albedo, while the undersampling error increased slowly and becomes the dominate term. The signal level of the measurements determines the undersampling error with τ_u being constant from spectrum to spectrum. That is, ΔXCO_2 increases with increasing surface albedo and decreases with increasing solar zenith angle (SZA). For $\Delta\lambda = 0.008$ nm, ΔXCO_2 varies from 0.85 to 0.9 ppm at SZA = 30° and from 0.35 to 0.45 ppm at SZA = 75°. For a negligible shift of 0.001 nm, the biases are typically less than 0.1 ppm. Figure 3b shows the conditions

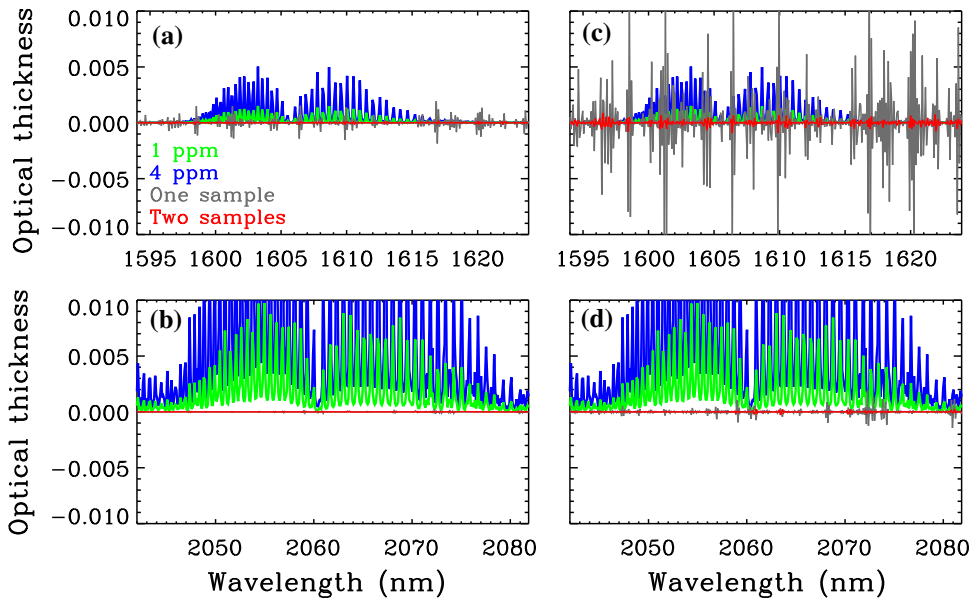

Fig. 2 Comparison of undersampling optical depth of one sample (*dark gray lines*) and two samples (*red lines*) with absorption optical depth of 1 (*green lines*) and 4 ppm (*blue lines*) CO_2 changes, for SZA = 30° and the vertical column density of CO_2 is 8.2×10^{21} molecules cm^{-3}. The relative wavelength shift between radiance and irradiance is (**a**, **b**) $\Delta\lambda = 0.001$ nm and (**c**, **d**) $\Delta\lambda = 0.008$ nm

when aerosol is present in the boundary layer. The scattering by aerosol modifies the light path of absorption and will increase G_y in contrast to the pure Rayleigh scattering atmosphere. For $\Delta\lambda = 0.008$ nm, ΔXCO_2 varies from 0.9 to 1.05 ppm at SZA = 30°. When the sampling rate is greater than two or a negligible shift of 0.001 nm, the ΔXCO_2 can be reduced significantly to less than 0.1 ppm for all cases.

Figure 3 also shows that the magnitude of error induced by undersampling error depends on the surface reflectance, SZA, and scattering properties in the atmosphere. That is, the undersampling error will result spatially in an artificial sources and sinks of CO_2. For example, the surface albedo in near infrared bands for soil is much larger than that for snow.

3 Comparison of scenarios

It has been demonstrated in Sect. 2 that spectra undersampling will add apparent noise in XCO_2 retrieved from synthetic TanSat measurements. Thus, the spectral sampling rate is, in turn, critical for instrument design as well as the development of XCO_2 retrieval algorithm.

3.1 Retrieval sensitivity analysis

The retrieval sensitivity to CO_2 depends on the spectral range, resolution, sampling rate, and uncertainties of measurement. Because the 1024-element detector is not available for TanSat, trade-offs among these parameters should be considered. Several feasible scenarios based on the 512-element detector have been proposed, as listed in Table 2; these include reduction of spectral resolution (scenario 1) or using narrower spectral regions (scenarios 2–5) in order to improve spectral sampling. Scenarios 2 and 3 contain a complete single branch of the full CO_2 absorption band, usually noted as the R and P branches in the wavenumber domain. Scenarios 4 and 5 extend scenarios 2 and 3 to wavelength coverage of 20 nm. All scenarios have spectral sampling rate larger than 2.0. We perform retrieval sensitivity analysis for these parameters for both pure Rayleigh atmosphere and with aerosol scattering. For three bands, the surface albedo is assumed to have a constant moderate value of 0.2.

As the DFS and XCO_2 error critically depend on the measurement SNR. The SNR is defined as

$$\mathrm{SNR} = (R \times F_{\mathrm{sol}})/I_{\mathrm{ref}} \times \mathrm{SNR}_{\mathrm{ref}} \times \Delta\lambda/\Delta\lambda_0, \quad (4)$$

where R is the normalized radiance modeled by VLIDORT, F_{sol} is the solar reference spectra, $\Delta\lambda$ is the sampling interval in nm, and $\Delta\lambda_0$ is the interval of TanSat preliminary instrument configuration. I_{ref} is the reference intensity and $\mathrm{SNR}_{\mathrm{ref}}$ is the SNR at I_{ref} and $\Delta\lambda_0$ as listed in Table 1. For example, the SNR is 250 for a radiance of 2.1×10^{12} photons^{-1} s^{-1} cm^{-2} sr^{-1} nm when $\Delta\lambda_0$ is 0.081 nm. This equation assumes that the SNR varies linearly with the energy entering the instrument and decouples the effects of spectral interval and signal-to-noise ratio. However, for a real instrument, it only reflects the readout noise.

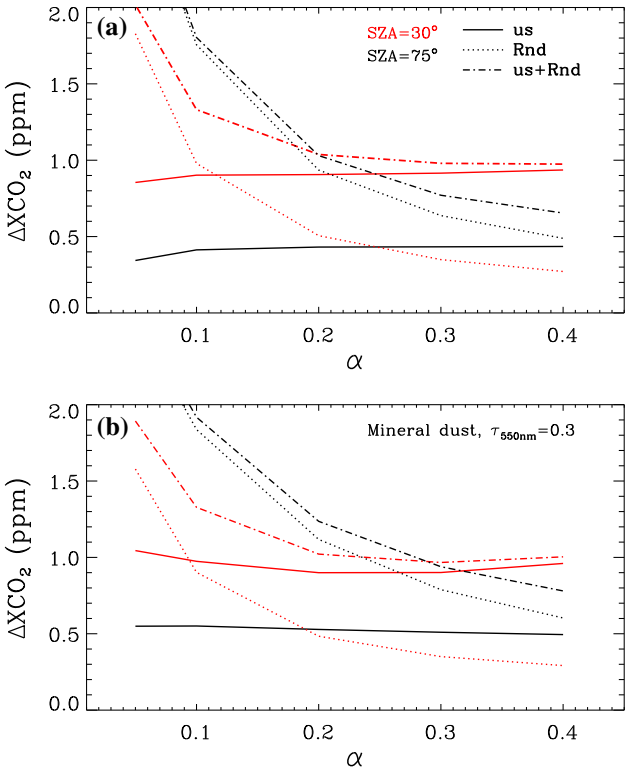

Fig. 3 Error in XCO_2 due to undersampling effect (us) in 1.61 μm band, random noise in measurements (Rnd), and square root of the two components as a function of surface albedo for SZA = 30° (*red*) and 75° (*black*) and $\Delta\lambda = 0.008$ nm: **a** Rayleigh scattering atmosphere and **b** mineral dust aerosol loading at 0–2 km with an optical depth of 0.3 at 550 nm

Table 2 Candidate FWHM, spectra interval, band coverage, and sampling rate for CO_2 weak band

Scenarios	FWHM (nm)	Interval (nm)	Band coverage (nm)	Sampling rate
0	0.081	0.030	1,594–1,624	2.7
1	0.162	0.060	1,594–1,624	2.7
2	0.081	0.024	1,594–1,606	3.4
3	0.081	0.036	1,606–1,624	2.3
4	0.081	0.041	1,594–1,614	2.0
5	0.081	0.041	1,604–1,624	2.0

For comparison, the values for 1024 elements detector is listed as scenario 0

Figure 4 shows the retrieval sensitivity to the instrument configuration under pure Rayleigh-scattering atmosphere. We use a linear estimate as the approximation of the nonlinear retrieval [10]. The column averaging kernels (CAK) is derived by summing all the rows of averaging kernel ($A = G_yK$), which describes the sensitivity of the retrieved XCO_2 to the real CO_2 profile. The trace of A describes the pieces of independent information that can be retrieved from the measured spectra, i.e. the degree of freedom for signal (DFS). The retrieval precision is the random noise error in the retrieved XCO_2.

As a reference, we take scenario 0, which is based on 1024-element detector with the same spectral resolution as the original configuration and a sampling rate of 2.7. The original configuration is noted as scenario −1. Different instrument configurations generally modify the XCO_2 sensitivity to the CO_2 changing in the middle troposphere (Fig. 4). Lower spectral resolution (scenario 1) has lower sensitivity to CO_2 but the increased spectral interval will enhance the effective signal-to-noise ratio in the measured spectra, thus increasing the DFS (Table 3). Although narrower band coverage (scenarios 2–5) contains fewer CO_2 absorption lines, it will decrease the DFS compared to the reference scenario 0. Scenarios 1 and 4 show the best sensitivity and smallest retrieval errors with values close to the reference scenario 0. It should be noted that even for the worst spectral resolution case, such as scenario 1, the DFS and retrieval precision do not change much compared with high-resolution cases. And the lower information content from the lower resolution can be offset by higher SNR. The DFS of elements in the state vector relates to aerosol and surface albedo are not changed.

3.2 Retrieval test with GOSAT data

Different instrument configurations do not significantly change CO_2 sensitivity, as shown in Fig. 4 and Table 3. However, for the retrieval of real satellite observed spectra, the auxiliary information (e.g. wavelength-dependent albedo and aerosol scattering properties) are not accurately known and need to be constrained by the measurements. To understand the effect of band coverage, we apply the TanSat CO_2 retrieval algorithm to GOSAT level 1B data [11] and compare the partial-band approaches (with spectral ranges same as scenarios 2–5) with the full-band approach, which refers to using all the measurements in the wavelength range 1,594–1,624 nm. The spectral resolution of GOSAT for three bands is similar to TanSat, so it is good dataset to test the TanSat retrieval algorithm with GOSAT level 1B data. The coincident pairs of GOSAT spectra and measurents at Lamont (a Total Carbon Column Observing Network (TCCON) station located at 36.6°N, 97.3°W) are selected according to the collocating criteria: 800 km in space, 1 h in time, and the AOD are typically less than 0.1. There are 33 coincident GOSAT spectra in total. The full-band approach has been well validated against the TCCON measurements with mean bias of 0.08 ppm and 1σ standard deviation of 2.3 ppm [11].

Figure 5 shows the scatter plot of partial-band retrievals versus full-band retrievals. There are significant biases with values from −0.79 to −1.34 ppm for scenarios 2, 3, and 5. For scenario 4, the partial-band approach agrees well with

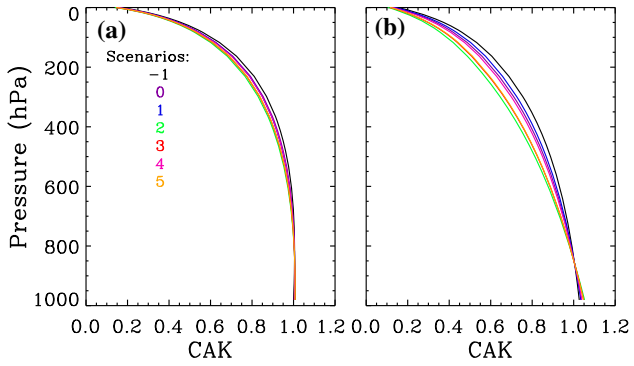

Fig. 4 The CAK for SZA = 30° (**a**) and 75° (**b**) for different scenarios listed in Table 2. For comparison, also plotted are the results of the original configuration (one sample) and the configuration based on a 1024-element detector (2.7 samples, scenario 0)

Table 3 Comparison of XCO_2 retrieval error and DFS of state vector elements for six scenarios

State vector	0	1	2	3	4	5
XCO_2 retrieval error (ppm)	0.35	0.36	0.40	0.39	0.36	0.39
XCO_2 DFS	1.81	1.80	1.76	1.78	1.81	1.78
H_2O profile DFS	1.63	1.30	1.56	1.25	1.46	1.22
Temperature DFS	2.89	2.29	2.54	2.44	2.64	2.41
Aerosol column DFS	0.72	0.71	0.72	0.71	0.72	0.71
Aerosol plume height DFS	0.60	0.44	0.53	0.41	0.53	0.42
Half width of aerosol plume DFS	0.11	0.05	0.09	0.04	0.08	0.05

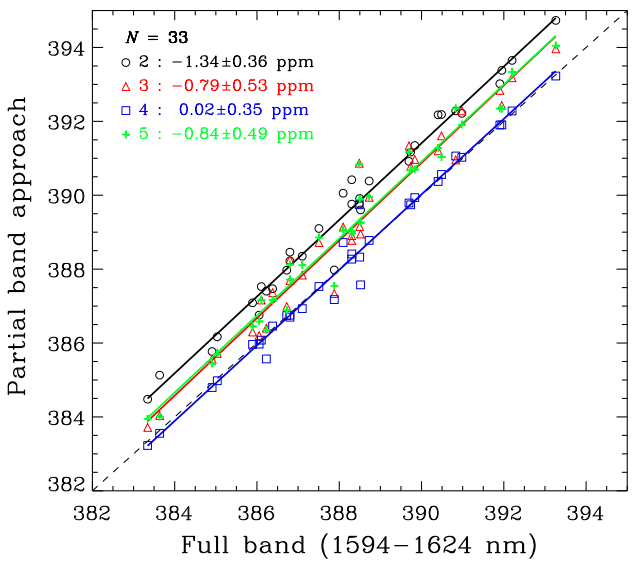

Fig. 5 Comparison of XCO_2 retrieved from GOSAT by the partial-band approaches that are proposed in Table 2 (i.e., scenarios 2, 3, 4, and 5) and the full-band approach. The *solid* and *dashed lines* denote the linear regression and 1:1 relationship, respectively. The number of ground pixels, mean bias, and 1σ standard deviation are also shown

the full-band approach with negligible bias of 0.02 ppm. The 1σ standard deviation is typically less than random noise error of a single sounding. The spectral range depended biases are caused by spectroscopic errors in the CO_2 spectroscopy as well as the possible effect of radiometric calibration of GOSAT. The TanSat retrieval algorithm retrieves a first-guess for the zero-order surface reflectance from the continuum part of the Sun-normalized radiance, and then fits a low-order polynomial to account for a continuous wavelength-dependent albedo. Therefore, for the retrieval algorithm to be self-constrained, it is essential to keep a broader band. The degradation of GOSAT spectral resolution by a factor of 2 does not increase the bias, the notable effect is increasing the standard deviation from 0.7 to 1.0 ppm [12].

4 Conclusion

We have evaluated the degree of spectral undersampling for the array detector-based spectrometer in the CO_2 1.61 and 2.06 μm absorption bands. In CO_2-weak band, the undersampling due to relative wavelength shift between the measured reference solar spectrum and Earth-viewing spectra significantly contaminate CO_2 signals. In CO_2 strong band, the undersampling-induced error is negligible. The spectral sampling rate is recommended to be greater than 2.0 pixels per FWHM to avoid undersampling. The addition of error in XCO_2 due to spectral undersampling can be up to 1 ppm. These errors are usually systematic and vary with surface albedo, SZA, and scattering properties in the atmosphere.

It is critical to improve the spectral sampling rate to avoid the undersampling effect. Retrieval sensitivity analysis shows that reduction of spectral resolution and the use of narrower spectral regions does not significantly change CO_2 sensitivity. GOSAT retrieval experiments show that, in the case of low aerosol loading, using the 1,594–1,614 nm (scenario 4 in Table 2) provides almost the same results as the full-band approach (1,594–1,624 nm) with bias less than 0.02 ppm and the degraded spectral resolution does not result in a worse comparison. Both scenario 1 and 4 are possible choices for the instrument. However, a narrower band will lose constraints on aerosol and surface albedo, especially in areas of higher aerosol loading and high CO_2 concentrations.

Similar to GOSAT and OCO-2, in the preliminary instrument configuration of TanSat, the wavelength ranges for three bands cover the complete gas absorption channels and continuum at both ends. The high-spectral resolution provides CO_2 information that can be distinguished from the measured spectra that interfered by absorption, scattering of other air molecules and particles, and surface

reflectors. This full-band approach provides direct constraints on the wavelength-dependent surface albedo and particle scattering in the measurements. To keep a broader band, the reduction of spectral resolution by a factor of two (scenario 1 in Table 2) will be the relatively easier way that only requires widening of entrance slit and performing little modification on the current optical framework.

Acknowledgments This work was supported by the Strategic Priority Research Program-Climate Change: Carbon Budget and Relevant Issues (XDA05040200), the National High-tech R&D Program of China (2011AA12A104) and the National Natural Science Foundation of China (41205018). Numerous discussions in the 1st TanSat International Workshop (esp. with Kelly Chance and Xiong Liu, Harvard-Smithsonian, Center for Astrophysics) are gratefully acknowledged for constructive suggestions. We thank David Crisp (JPL) and Heinrich Bovensmann (University of Bremen) for useful comments and discussions. We also thank the GOSAT science teams for providing L1B products.

References

1. Bovensmann H, Burrows JP, Buchwitz M et al (1999) SCIAMACHY: mission objectives and measurement modes. J Atmos Sci 56:127–150
2. Yokota T, Yoshida Y, Eguchi N et al (2009) Global concentrations of CO_2 and CH_4 retrieved from GOSAT: first preliminary results. SOLA 5:160–163
3. O'Dell CW, Connor B, Bosch H et al (2012) The ACOS CO_2 retrieval algorithm—Part 1: description and validation against synthetic observations. Atmos Meas Tech 5:99–121
4. Chance K, Kurosu TP, Sioris CE (2005) Undersampling correction for array detector-based satellite spectrometers. Appl Opt 44:1296–1304
5. Oshchepkov S, Bril A, Yokota T (2009) An improved photon path length probability density function based radiative transfer model for space based observation of greenhouse gases. J Geophys Res 114:D19207
6. Bosch H, Toon GC, Sen B et al (2006) Spacebased near-infrared CO_2 measurements: testing the Orbiting Carbon Observatory retrieval algorithm and validation concept using SCIAMACHY observations over Park Falls, Wisconsin. J Geophys Res 111:23302
7. Butz A, Guerlet S, Hasekamp O et al (2011) Toward accurate CO_2 and CH_4 observations from GOSAT. Geophys Res Lett 38:L14812
8. Yoshida Y, Ota Y, Eguchi N et al (2011) Retrieval algorithm for CO_2 and CH_4 column abundances from short-wavelength infrared spectral observations by the greenhouse gases observing satellite. Atmos Meas Tech 4:717–734
9. Liu Y, Duan M, Cai Z et al (2012) Chinese carbon dioxide satellite (TanSat) status and plans. AGU fall meeting, San Francisco
10. Cai Z, Liu Y, Yang D (2013) Sensitivity studies for the retrieval of XCO_2 from simulated Chinese Carbon Satellite (TanSat) measurements: A linear error analysis. Sci China Ser D Earth Sci. doi:10.1007/s11430-013-4707-1
11. Liu Y, Yang DX, Cai ZN (2013) A retrieval algorithm for TanSat XCO_2 observation: retrieval experiments using GOSAT data. Chin Sci Bull 58:1520–1523
12. Galli A, Landgraf J (2013) Reduction of spectral resolution and sampling: application to GOSAT. SRON-TROPSC-TN-2013-XX